

# $\text{Li}_4\text{Ti}_{2.5}\text{Cr}_{2.5}\text{O}_{12}$ as anode material for lithium battery

M. Ganesan

Received: 15 June 2007 / Revised: 6 August 2007 / Accepted: 2 October 2007 / Published online: 24 October 2007  
© Springer-Verlag 2007

**Abstract** Chromium-substituted  $\text{Li}_4\text{Ti}_5\text{O}_{12}$  has been investigated as a negative electrode for future lithium batteries. It has been synthesized by a solid-state method followed by quenching leading to a micron-sized material. The minimum formation temperature of  $\text{Li}_4\text{Ti}_{2.5}\text{Cr}_{2.5}\text{O}_{12}$  was found to be around 600 °C using thermogravimetric and differential thermal analysis. X-ray diffraction, scanning electron microscopy, cyclic voltammetry (CV), impedance spectroscopy, and charge–discharge cycling were used to evaluate the synthesized  $\text{Li}_4\text{Ti}_{2.5}\text{Cr}_{2.5}\text{O}_{12}$ . The particle size of the powder was around 2–4  $\mu\text{m}$ . CV studies reveal a shift in the deintercalation potential by about 40 mV, i.e., from 1.54 V for  $\text{Li}_4\text{Ti}_5\text{O}_{12}$  to 1.5 V for  $\text{Li}_4\text{Ti}_{2.5}\text{Cr}_{2.5}\text{O}_{12}$ . High-rate cyclability was exhibited by  $\text{Li}_4\text{Ti}_{2.5}\text{Cr}_{2.5}\text{O}_{12}$  (up to 5 °C) compared to the parent compound. The conduction mechanism of the compound was examined in terms of the dielectric constant and dissipation factor. The relaxation time has been evaluated and was found to be 0.07 ms. The mobility was found to be  $5.133 \times 10^{-6} \text{ cm}^2 \text{ V}^{-1} \text{ s}^{-1}$ .

**Keywords**  $\text{Li}_4\text{Ti}_5\text{O}_{12}$  ·  $\text{Li}_4\text{Ti}_{2.5}\text{Cr}_{2.5}\text{O}_{12}$  · Quench method · Cyclic voltammetry · a.c. impedance · Charge–discharge · Dielectric · Relaxation time · Mobility

## Introduction

Rechargeable energy storage devices are being used in increasing numbers in several consumer applications, such

as hybrid vehicles, wireless communication devices, uninterrupted power sources, and power tools. Lightweight, compact, high power, and an energy density storage device with excellent charging rate capability are desired for the above applications. Lead acid and Ni–Cd batteries, which are presently being used for these applications, suffer from low cycle life, poor charge retention, limited charging rate capabilities, and environmental issues. Li-ion batteries overcome such issues.

In general, the anode material for Li-ion batteries are graphite, carbon, etc. Recently,  $\text{Li}_4\text{Ti}_5\text{O}_{12}$  is considered as a suitable anode material for both high-power Li-ion batteries and asymmetric hybrid devices because of its excellent structural stability (no structural change during charging and discharging) and no risk of lithium plating during the fast charge rate, as the reduction potential of  $\text{Li}_4\text{Ti}_5\text{O}_{12}$  is 1.5 V vs  $\text{Li}^+/\text{Li}$  [1–10].

Despite of the excellent performance, the electronic conductivity of the material is extremely low because of its insulator properties. Further, the voltage is rather high for utilization, as the negative electrode is more than 1.5 V vs  $\text{Li}^+/\text{Li}$ . To improve the electrical conductivity of this material and also to bring down the working potential recent studies have been focused. Chen et al. [11] reported the substitution of  $\text{Mg}^{2+}$  ions for  $\text{Li}^+$  ions in  $\text{Li}_4\text{Ti}_5\text{O}_{12}$ . It is generally believed that a transition metal sharing the tetrahedral sites with the lithium ions in spinel oxides inhibit the lithium ion diffusion through them during intercalation and decline their performance during charge–discharge cycling. Robertson et al. [12, 13] reported the effect of replacing some  $\text{Ti}^{4+}$  with  $\text{M}^{3+}$  (transition metal  $3\text{M}^{3+} = 2\text{Ti}^{4+} + \text{Li}^+$ ,  $\text{M} = \text{Fe}, \text{Cr}, \text{Ni}$ ) in  $\text{Li}_4\text{Ti}_5\text{O}_{12}$  with the aim to synthesize low-working-voltage materials, working at less than 1 V vs  $\text{Li}^+/\text{Li}$ .  $\text{Cr}^{3+}$  is chosen as an alternative dopant because its ionic radii is similar to  $\text{Ti}^{4+}$  and it prefers

M. Ganesan (✉)  
Electrochemical Energy Systems Division,  
Central Electro Chemical Research Institute,  
Karaikudi 630006, India  
e-mail: mgshan2002@yahoo.co.in

octahedral coordination. Further, rate capability was increased by the substitution of Cr in  $\text{Li}_{1+x}\text{M}_{1-3x}\text{Ti}_{1+2x}\text{O}_4$ , which was studied by Sun et al. [14]. The partial substitution of Cr in  $\text{Li}_{1+x}\text{M}_{1-3x}\text{Ti}_{1+2x}\text{O}_4$  with  $x=0.3$  has got beneficial effect in reducing the reduction voltage by 0.09 V. Therefore, we have focused our study on the effect of higher Cr substitution in  $\text{Li}_4\text{Ti}_5\text{O}_{12}$ .

The results obtained with chromium-substituted  $\text{Li}_4\text{Ti}_5\text{O}_{12}$  synthesized by a solid-state high-temperature method followed by quenching and its characterization by thermal analysis, particle size distribution, X-ray diffraction (XRD), and scanning electron microscopy (SEM) have been reported. Electrochemical charge–discharge, cyclic voltammetry (CV), and impedance have also been done, and results are presented in this communication.

## Experimental

Synthesis of  $\text{Li}_4\text{Ti}_5\text{O}_{12}$  was carried out with high-purity starting materials such as  $\text{TiO}_2$  (E. Merck),  $\text{Li}_2\text{CO}_3$  (E. Merck), and  $\text{Cr}_2\text{O}_3$  (E. Merck).  $\text{TiO}_2$ ,  $\text{Li}_2\text{CO}_3$ , and  $\text{Cr}_2\text{O}_3$  was initially ball milled for 15 h before mixing stoichiometrically. A mixture corresponding to the composition  $\text{Li}_4\text{Ti}_{2.5}\text{Cr}_{2.5}\text{O}_{12}$  was weighed and ball milled with acetone at room temperature for 15 h. The powders were dried at 90 °C for 8 h and fired at 900 °C for 24 h. The molten mass was suddenly quenched in ice-cold medium and reground. The structure and morphology of the synthesized oxide powders was characterized by several techniques. XRD data were collected using a JEOL-JDX 8030 X-ray diffractometer,  $\lambda=1.5406$  Å using nickel-filtered  $\text{Cu}_{K\alpha}$ . Particle size distribution was carried out using Horiba LA -910 Laser scattering particle size analyzer. Thermogravimetric and differential thermal analysis (TG/DTA) were performed using STA 1500 Thermal analyzer from 20 to 900 °C at a heating rate of 20 °C  $\text{min}^{-1}$ . Surface morphology of the compound was characterized by Hitachi S 3000H Scanning Electron Microscope. The Brunauer–Emmett–Teller (BET) surface area of the prepared material was determined from nitrogen adsorption isotherm at 77 K (Quanta Chrome Nova 1000, USA).

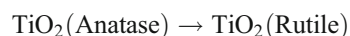
Electrochemical studies were carried out using a 2016-coin cell assembled inside a glove box. Autolab PGSTAT 30, controlled by the GPES—4.9 software, was used. The electrolyte solution used was an ethylene carbonate/dimethyl carbonate (1:1) mixture with 1 M  $\text{LiPF}_6$ . The reference and auxiliary electrodes were Li metal; hence, potentials are referred to the  $\text{Li}/\text{Li}^+$  reference electrode. The anode was prepared by coating  $\text{Li}_4\text{Ti}_{2.5}\text{Cr}_{2.5}\text{O}_{12}$  (85%) mixed with 10% of acetylene black and 5% polyvinylidene fluoride as binder over aluminum foil. Impedance spectroscopy was carried out in the frequency range 1 mHz–100 kHz using Autolab

PGSTAT 30. Dielectric constant, dissipation factor, mobility, and relaxation time were evaluated from impedance parameters. A computer-controlled Bitrode USA life cycle tester was used for cycle tests at constant current.

## Results and discussion

### Thermogravimetric and differential thermal analysis

Figure 1 shows the TG/DTA analysis (from 20 to 900 °C) of Cr-substituted  $\text{Li}_4\text{Ti}_5\text{O}_{12}$  obtained from high-temperature solid-state reactions of  $\text{TiO}_2$ ,  $\text{Li}_2\text{CO}_3$ , and  $\text{Cr}_2\text{O}_3$ . It can be seen from the figure that the  $\text{Li}_4\text{Ti}_{2.5}\text{Cr}_{2.5}\text{O}_{12}$  precursor follows almost the same kinetics of formation as that of its parent compound  $\text{Li}_4\text{Ti}_5\text{O}_{12}$  and the formation of the  $\text{Li}_4\text{Ti}_{2.5}\text{Cr}_{2.5}\text{O}_{12}$  takes place at around 800 °C. From the TG curve, it was found that the formation of  $\text{Li}_4\text{Ti}_{2.5}\text{Cr}_{2.5}\text{O}_{12}$  follows two main regions. The two distinct steps of weight losses observed on the TG curve of the precursor powder is indicative of this. The total mass loss was 39%. The first step up to 250 °C is obviously due to the vaporization of water and loss of carbonates. The second step in the temperature range 480–530 °C indicates the phase change reaction of  $\text{TiO}_2$  and the onset of formation of  $\text{Li}_4\text{Ti}_{2.5}\text{Cr}_{2.5}\text{O}_{12}$ . The two endothermic peaks around 215 and 500 °C on the DTA curve can be assigned to the decomposition of  $\text{Cr}_2\text{O}_3$  and the phase-change reaction, followed by the formation of  $\text{Li}_4\text{Ti}_{2.5}\text{Cr}_{2.5}\text{O}_{12}$ . An exothermic peak at 400 °C can be assigned to the phase transformation of  $\text{Cr}_2\text{O}_3$  to CrO. A weak endothermic peak that appeared around 500 °C in the DTA curve can be ascribed to the anatase–rutile transformation before the formation of the spinel phase  $\text{Li}_4\text{Ti}_{2.5}\text{Cr}_{2.5}\text{O}_{12}$ :



The minimum formation temperature required for the synthesis of  $\text{Li}_4\text{Ti}_{2.5}\text{Cr}_{2.5}\text{O}_{12}$  is around 600 °C, and for

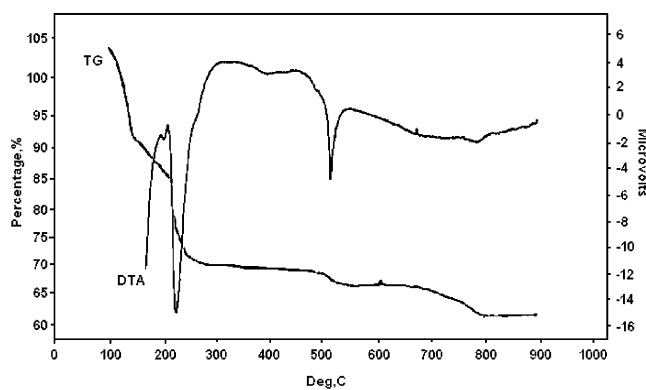
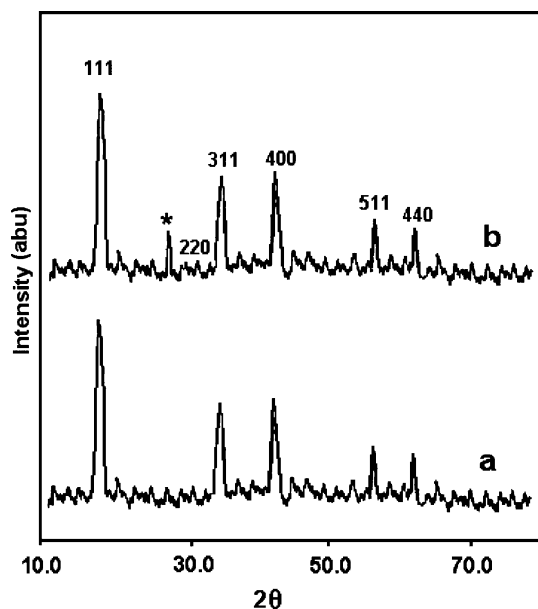


Fig. 1 TG/DTA curve for  $\text{Li}_4\text{Ti}_{2.5}\text{Cr}_{2.5}\text{O}_{12}$



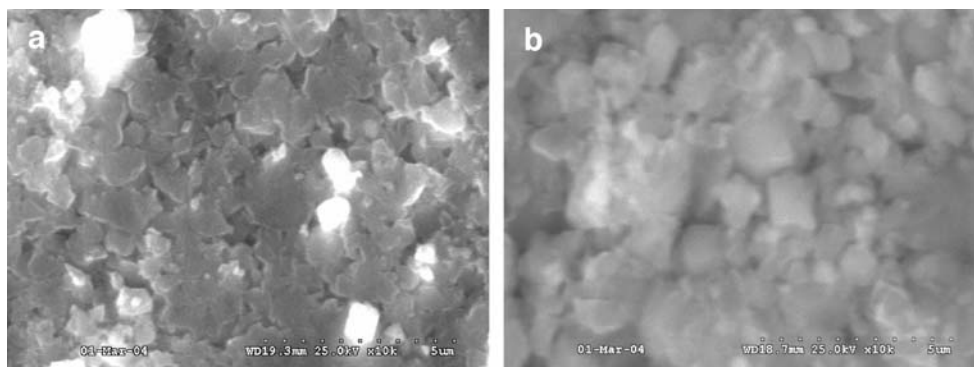
**Fig. 2** XRD pattern. *a*  $\text{Li}_4\text{Ti}_5\text{O}_{12}$ , *b*  $\text{Li}_4\text{Ti}_{2.5}\text{Cr}_{2.5}\text{O}_{12}$ , asterisk,  $\text{TiO}_2$  Peak

getting phase-pure  $\text{Li}_4\text{Ti}_{2.5}\text{Cr}_{2.5}\text{O}_{12}$ , the sample was heated up to 800 °C.

#### X-Ray diffraction

Figure 2 shows the XRD patterns of the  $\text{Li}_4\text{Ti}_{2.5}\text{Cr}_{2.5}\text{O}_{12}$  and  $\text{Li}_4\text{Ti}_5\text{O}_{12}$  powders. The XRD patterns shown in Fig. 2 correlates well with that reported for  $\text{Li}_4\text{Ti}_5\text{O}_{12}$  having a spinel framework structure. The XRD pattern reveals all the characteristic diffraction peaks corresponding to the (111), (311), (400), (511), and (440) diffraction planes of the spinel  $\text{Li}_4\text{Ti}_5\text{O}_{12}$  crystal. A small amount of characteristic principal peak of  $\text{TiO}_2$  localized at  $2\theta$  Bragg angle 25.280 in  $\text{Li}_4\text{Ti}_{2.5}\text{Cr}_{2.5}\text{O}_{12}$  indicates that the Cr cations are located at the octahedral site (16c). The absence of the (220) peak strongly suggests that there is no transition metal on the tetrahedral sites, and it is associated with the co-migration of tetrahedrally coordinated lithium and chromium ions to the octahedral 16c sites. Further, the ionic radius of  $\text{Cr}^{3+}$  (0.62 Å) is nearly the same as that of  $\text{Ti}^{4+}$  (0.61 Å).

**Fig. 3** **a** SEM picture of  $\text{Li}_4\text{Ti}_5\text{O}_{12}$ ; **b** SEM picture of  $\text{Li}_4\text{Ti}_{2.5}\text{Cr}_{2.5}\text{O}_{12}$



Therefore, it was suggested that the Cr cations enter the spinel structure. The sharpness of the main peak that appeared at  $2\theta=18.36^\circ$  indicates a high crystallinity of the synthesized powder. As illustrated by DTA, the  $\text{Li}_4\text{Ti}_{2.5}\text{Cr}_{2.5}\text{O}_{12}$  crystal phase began to form at 600 °C, and it is completed at 800 °C, which is inferred by the absence of any additional peak in the synthesized compound. The lattice parameter of the synthesized compound was 8.350 Å, which also agree well with the literature, and it has a defective spinel framework structure with  $a=8.367$  Å. This is in agreement with Ohzuku et al. (8.367 Å) [9] and Colbow et al. (8.365 Å) [10]. This value is also similar to the lattice constant of 0.8359 nm calculated from the JCP2 CAT pattern (PDF.no-26-1198). The intensities of the main peak in Fig. 2 corresponds to the space group of  $\text{Fd}\bar{3}\text{M}$ , where lithium ions are located at the tetrahedral 8(a) sites and tetravalent titanium ions at 3(d), and the lithium ions are randomly distributed at octahedral 16(d) sites by the ratio of  $\text{Li}/\text{Ti}=1/5$ , while oxygen ions are located at 32(a) sites. According to the Reitveld refinement carried out by Robertson et al. [12] proved that the doped  $\text{Li}_4\text{Ti}_5\text{O}_{12}$  share the 16d octahedral site, which is in agreement with our XRD parameters.

#### SEM and particle size distribution

SEM images of  $\text{Li}_4\text{Ti}_5\text{O}_{12}$  and  $\text{Li}_4\text{Ti}_{2.5}\text{Cr}_{2.5}\text{O}_{12}$  crystals are shown in Fig. 3a and b. It is apparent that  $\text{Li}_4\text{Ti}_5\text{O}_{12}$  and  $\text{Li}_4\text{Ti}_{2.5}\text{Cr}_{2.5}\text{O}_{12}$  exhibits regular uniform particles with good dispersivity. From the figure, it appears that  $\text{Li}_4\text{Ti}_5\text{O}_{12}$  and  $\text{Li}_4\text{Ti}_{2.5}\text{Cr}_{2.5}\text{O}_{12}$  display evenly distributed fine particles with small agglomerates.

The particle size by SEM was reasonably in agreement with the values calculated from the equation

$$d_p = 6/\rho S_{\text{BET}} \quad (1)$$

where  $d$  is the particle size,  $\rho$  is the density, and  $S_{\text{BET}}$  is the surface area of the particle estimated from the BET area.

The average particle size was estimated by assuming nonporous spherical grains of a density  $\rho=3.5$  g  $\text{cm}^{-3}$ . The average particle size of  $\text{Li}_4\text{Ti}_5\text{O}_{12}$  is about 280 nm and for  $\text{Li}_4\text{Ti}_{2.5}\text{Cr}_{2.5}\text{O}_{12}$  is about 413 nm, respectively.

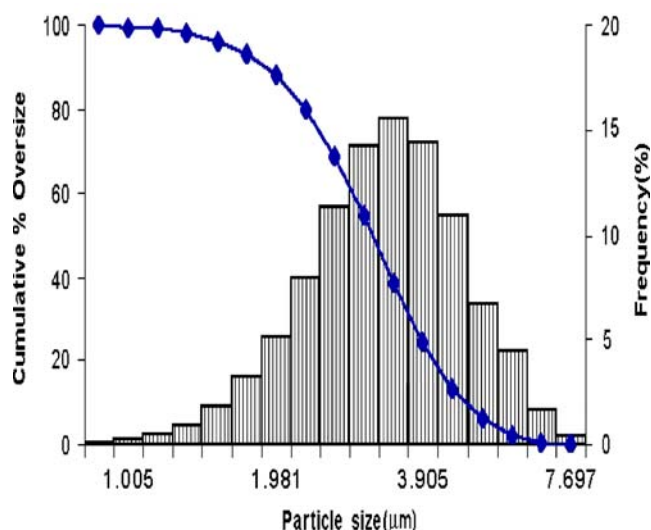


**Fig. 4** Particle size distribution of  $\text{Li}_4\text{Ti}_{2.5}\text{Cr}_{2.5}\text{O}_{12}$

The dimensions of  $\text{Li}_4\text{Ti}_5\text{O}_{12}$  and  $\text{Li}_4\text{Ti}_{2.5}\text{Cr}_{2.5}\text{O}_{12}$  particles were obtained from the full width half maxima of peaks observed in Fig. 2 using the Scherrer formula:

$$D = \beta\lambda / B \cos \theta \quad (2)$$

Where  $D_{hkl}$  is the linear dimension of the coherent diffraction along a direction normal to the diffraction plane ( $hkl$ ),  $\lambda$  is the X-ray wavelength (1.5418 Å),  $\beta$  is the crystal shape constant (0.89),  $\theta$  is the reflection angle of the peak, and  $B$  is the corrected full width at half maximum (FWHM) of the peak in radians. Calculated from the width of the XRD reflection peaks, the crystallite size of  $\text{Li}_4\text{Ti}_5\text{O}_{12}$

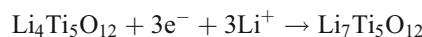
particles are 240 (111), 337 (311), 620 (400), and 200 nm (440), respectively, and for  $\text{Li}_4\text{Ti}_{2.5}\text{Cr}_{2.5}\text{O}_{12}$  are 240 (111), 337 (311), 620 (400), and 200 nm (440), respectively.

From Fig. 4, the average particle size of  $\text{Li}_4\text{Ti}_{2.5}\text{Cr}_{2.5}\text{O}_{12}$  determined by the laser diffraction-scattering method is 3.46  $\mu\text{m}$ , exhibiting the coefficient of variation on a volume basis. The particle size of the powder was uniformly distributed between 2 and 4  $\mu\text{m}$ . The specific surface area was determined by the BET method, and it is 4.15  $\text{m}^2 \text{g}^{-1}$ .

#### Electrochemical studies

##### Cyclic voltammetry studies

The electrochemical properties of  $\text{Li}_4\text{Ti}_{2.5}\text{Cr}_{2.5}\text{O}_{12}$  sample was evaluated with a CV at 20  $\text{mV s}^{-1}$  in a mixed solvent of ethylene carbonate and dimethyl carbonate containing 1.0  $\text{mol dm}^{-3}$   $\text{LiPF}_6$ . Figure 5a and b shows a cyclic voltammetry of  $\text{Li}_4\text{Ti}_5\text{O}_{12}$  and  $\text{Li}_4\text{Ti}_{2.5}\text{Cr}_{2.5}\text{O}_{12}$  sample. The voltage was scanned from 1.2 to 2.5 V and back at a scan rate 20  $\text{mV s}^{-1}$ . As per the following reaction



lithium insertion should occur at 1.54 V and extraction at 1.6 V for phase-pure  $\text{Li}_4\text{Ti}_5\text{O}_{12}$ ; CV studies indicated that the unsubstituted  $\text{Li}_4\text{Ti}_5\text{O}_{12}$  compound (Fig 5a) is phase pure and free from anatase phase, which is established by the absence of peaks at 1.75 and 2.0 V vs  $\text{Li/Li}^+$  [15], but in the  $\text{Li}_4\text{Ti}_{2.5}\text{Cr}_{2.5}\text{O}_{12}$  compound, the peaks are observed at 1.75 and 2.0 V (Fig 5b) indicating the presence of  $\text{TiO}_2$  (anatase) [15], which is in agreement with XRD data also.

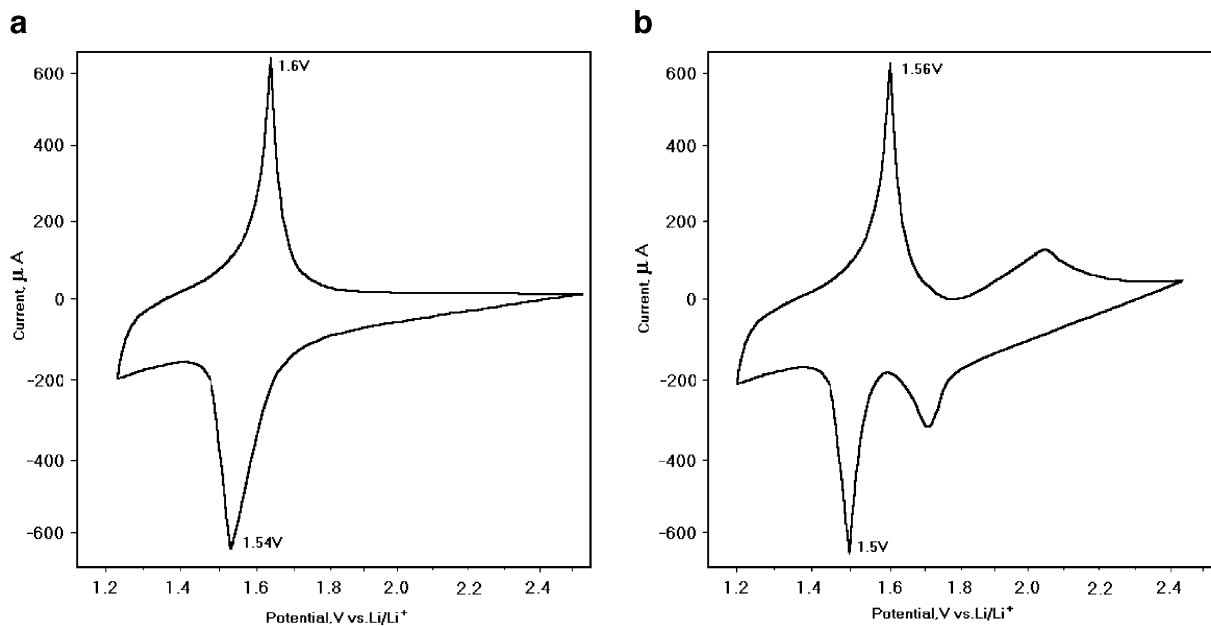


**Fig. 5** a Cyclic voltammogram of  $\text{Li}_4\text{Ti}_5\text{O}_{12}$ ; b cyclic voltammogram of  $\text{Li}_4\text{Ti}_{2.5}\text{Cr}_{2.5}\text{O}_{12}$

The oxidation and reduction potential for the  $\text{Li}_4\text{Ti}_{2.5}\text{Cr}_{2.5}\text{O}_{12}$  compound is slightly lower than  $\text{Li}_4\text{Ti}_5\text{O}_{12}$ , i.e., 1.56 and 1.5 V, respectively. This deviation in electrochemical behavior observed for the  $\text{Li}_4\text{Ti}_{2.5}\text{Cr}_{2.5}\text{O}_{12}$  compound is due to the presence of Cr. This is in good agreement with Robertson et al. [12].

The peaks are sharp, indicating phase-pure nature of the materials, and the obtained cyclic voltammogram was in good agreement with that of previous works, synthesized using different methods [16–20].

*Charge–discharge studies*

Figure 6 shows the charge–discharge behavior for both  $\text{Li}_4\text{Ti}_{2.5}\text{Cr}_{2.5}\text{O}_{12}$  and  $\text{Li}_4\text{Ti}_5\text{O}_{12}$  at  $20 \mu\text{A cm}^{-2}$  in a mixed solvent of ethylene carbonate and diethyl carbonate containing  $1.0 \text{ mol dm}^{-3} \text{ LiPF}_6$ . It was found that the discharge capacity of the  $\text{Li}_4\text{Ti}_{2.5}\text{Cr}_{2.5}\text{O}_{12}$  was lower than that of the  $\text{Li}_4\text{Ti}_5\text{O}_{12}$ . The discharge and charge curves were very flat, and their working potentials were around 1.55 V. This potential range corresponds to the free energy change of  $\text{Li}_4\text{Ti}_5\text{O}_{12}$  as reported earlier [17, 18, 20–22]. The discharge test was carried out between 2.5 and 1.0 V, and the voltage was dropped quickly down to below 2 V and further decreases as the reaction proceed until the voltage reaches about 1.51 V, after which the voltage was almost constant displaying the characteristic discharge plateau for  $\text{Li}_4\text{Ti}_5\text{O}_{12}$ . This initial rapid loss in capacity has already been observed for sol–gel-derived  $\text{Li}_4\text{Ti}_5\text{O}_{12}$  [23] and for the material prepared with the high-energy ball-milling method [24]. The initial discharge capacities of these powder decrease with Cr substitution in the active material because of a decrease in the amount of extractable  $\text{Li}^+$  ion

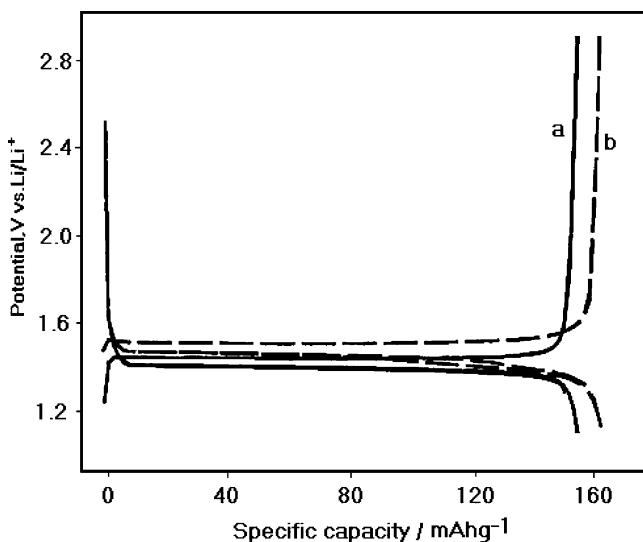


**Fig. 6** Charge–discharge curve at 2C rate. *a*  $\text{Li}_4\text{Ti}_5\text{O}_{12}$ , *b*  $\text{Li}_4\text{Ti}_{2.5}\text{Cr}_{2.5}\text{O}_{12}$

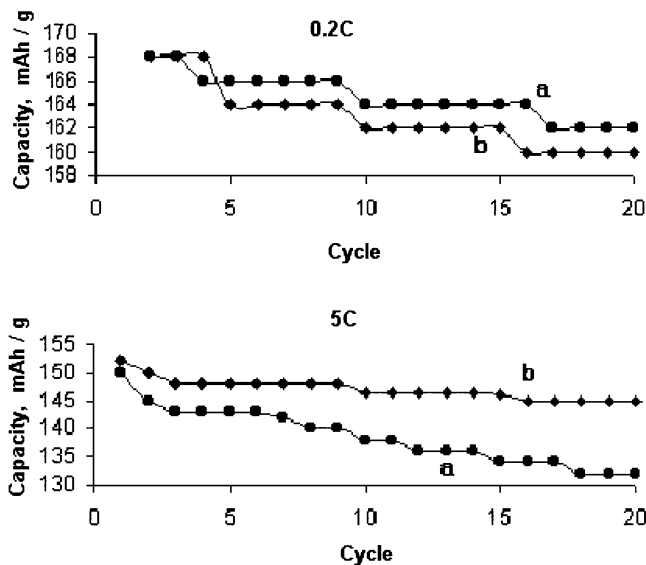


**Fig. 7** Charge–discharge curve at 0.2C and 5C rate. *a*  $\text{Li}_4\text{Ti}_5\text{O}_{12}$ , *b*  $\text{Li}_4\text{Ti}_{2.5}\text{Cr}_{2.5}\text{O}_{12}$

in the spinel. The discharge capacity of  $\text{Li}_4\text{Ti}_{2.5}\text{Cr}_{2.5}\text{O}_{12}/\text{Li}$  cell at various *C* rates is presented in Fig 7.

From Table 1, we could easily find that the reversible capacity of  $\text{Li}_4\text{Ti}_{2.5}\text{Cr}_{2.5}\text{O}_{12}$  was slightly lower with lesser capacity loss in comparison with the unsubstituted one. However, when the charge–discharge rate increased, the discharge capacities of the  $\text{Li}_4\text{Ti}_{2.5}\text{Cr}_{2.5}\text{O}_{12}$  became much higher than those of the unsubstituted  $\text{Li}_4\text{Ti}_5\text{O}_{12}$ . It is clear that synthesised compound have better results when compared to reports available [14].

*Impedance studies*

The impedance of the electrode can be interpreted in terms of a single circuit in which a resistance–capacitance network (*R–C*) is connected in series with the bulk electrolyte resistance  $R_s$ . In the  $R_c$  network,  $R_{ct}$  is the charge transfer resistance representing the faradic process and  $C_{dl}$  as the double-layer capacitance.  $R_{ct}$  is connected in series with an element that takes into account for the finite diffusion length  $Z_F$ . At very

**Table 1** Capacity of  $\text{Li}_4\text{Ti}_5\text{O}_{12}$  and  $\text{Li}_4\text{Ti}_{2.5}\text{Cr}_{2.5}\text{O}_{12}$  at various *C* rates

		0.2C	0.5C	1C	2C	5C
$\text{Li}_4\text{Ti}_5\text{O}_{12}$	1st cycle	176	170	168	154	150
	20th cycle	166	162	160	144	132
	Capacity fade (%)	1.0	0.8	0.8	1.0	1.8
$\text{Li}_4\text{Ti}_{2.5}\text{Cr}_{2.5}\text{O}_{12}$	1st cycle	168	164	160	156	152
	20th cycle	160	158	156	151	146
	Capacity fade (%)	0.80	0.6	0.4	0.50	0.6

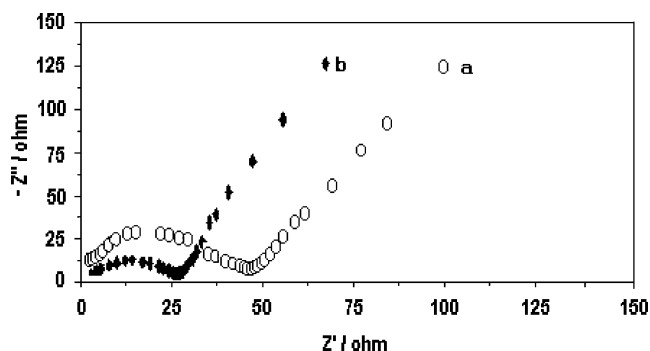


Fig. 8 Impedance spectra. *a*  $\text{Li}_4\text{Ti}_5\text{O}_{12}$ , *b*  $\text{Li}_4\text{Ti}_{2.5}\text{Cr}_{2.5}\text{O}_{12}$

low frequencies, the plot gives rise to a straight line. Fig. 8 shows a complex impedance diagram for  $\text{Li}_4\text{Ti}_5\text{O}_{12}$  and  $\text{Li}_4\text{Ti}_{2.5}\text{Cr}_{2.5}\text{O}_{12}$  obtained in the frequency range  $10^4$ – $10^{-3}$  Hz. Figure 8 shows a semicircle and a straight line obtained in the high and intermediate frequencies. This straight line corresponds to the Warburg impedance, which is due to a semi-infinite diffusion, and the vertical line is due to a finite diffusion of  $\text{Li}^+$  ion. The diameter of the semicircle appearing at a higher frequency region corresponds to a charge transfer resistance. The chemical diffusion coefficient was determined as reported by Cabanel et al. [25] from the equation  $D = \pi f l^2 / 1.94$ , where  $f$  is transition frequency,  $l$  is the thickness of the material or film, and  $D$  is the chemical diffusion coefficient. The chemical diffusion coefficient obtained from the above equation for the unsubstituted and Cr-substituted  $\text{Li}_4\text{Ti}_5\text{O}_{12}$  was  $0.14 \times 10^{-14}$  and  $3.1 \times 10^{-9} \text{ cm}^2 \text{ s}^{-1}$ , respectively. It is well in agreement with the reported values [26]. Thus, the diffusion was increased by the substitution of Cr in  $\text{Li}_4\text{Ti}_5\text{O}_{12}$  [14].

Furthermore, the  $\text{Li}_4\text{Ti}_{2.5}\text{Cr}_{2.5}\text{O}_{12}$  and  $\text{Li}_4\text{Ti}_5\text{O}_{12}$  system displays only one semicircle, and this suggests that there is no passivation observed. This suggests that  $\text{Li}_4\text{Ti}_{2.5}\text{Cr}_{2.5}\text{O}_{12}$  and  $\text{Li}_4\text{Ti}_5\text{O}_{12}$  can be considered as a passivation-free electrode [21]. The conductivity of the specimen was determined from the alternating current impedance spectroscopy at ambient temperature using the formula  $\sigma = d/AR$ , where  $d$  is the thickness of the electrode,  $A$  is the surface area of the electrode, and  $R$  is the resistance. The conductivities of  $\text{Li}_4\text{Ti}_5\text{O}_{12}$  and  $\text{Li}_4\text{Ti}_{2.5}\text{Cr}_{2.5}\text{O}_{12}$  are found to be  $5.3 \times 10^{-4}$  and  $9.8 \times 10^{-4} \text{ S/cm}$ , respectively.

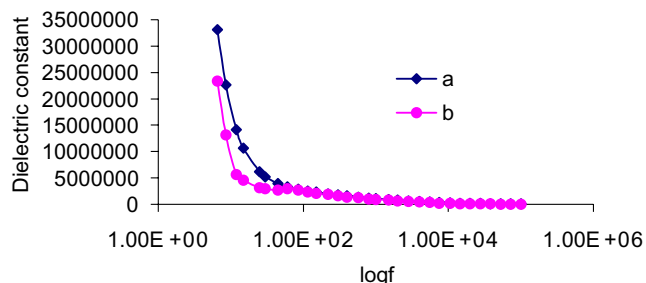


Fig. 9  $\log f$  vs dielectric constant. *a*  $\text{Li}_4\text{Ti}_5\text{O}_{12}$ , *b*  $\text{Li}_4\text{Ti}_{2.5}\text{Cr}_{2.5}\text{O}_{12}$

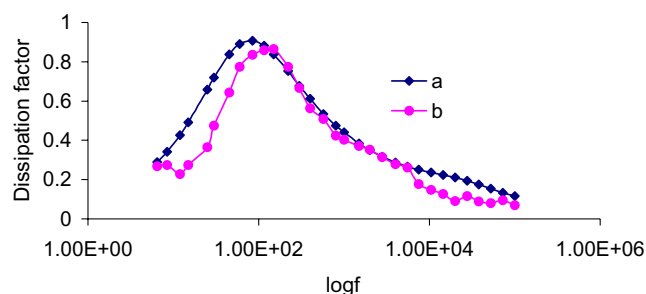


Fig. 10  $\log f$  vs dissipation factor. *a*  $\text{Li}_4\text{Ti}_5\text{O}_{12}$ , *b*  $\text{Li}_4\text{Ti}_{2.5}\text{Cr}_{2.5}\text{O}_{12}$

To elucidate the conduction mechanism in the synthesized compounds, dielectric properties were calculated. Dielectric constant values as a function of frequency at room temperature are shown in Fig. 9. The dielectric constant  $\epsilon$  were calculated from the following equation  $\epsilon = C t / \epsilon_0 A$ , where  $C$  is the capacitance,  $\epsilon_0$  is the permittivity of empty space,  $t$  the film thickness, and  $A$  is the area of the electrode. The dielectric constant was found to increase rapidly at low frequencies and stay more or less constant at higher frequencies.  $\text{Li}_4\text{Ti}_5\text{O}_{12}$  shows low-frequency dispersion of the dielectric constant, which is attributed to the grain-to-grain contact as reported. The dielectric constant is relatively stable up to a frequency of about 1,000 Hz, after which it increases abruptly at a small frequency. The  $D$  vs  $\log f$  plots of the sample is shown in Fig. 10. From the figure, it is clear that  $D$  decreases initially and after a particular frequency starts increasing and attains maximum, then decreases again with increasing frequency. From the peak obtained and using the relation  $\omega\tau = 1$  ( $\omega$ , the angular frequency is equal to  $2\pi f$ ,  $f$  being the frequency [Hz] and  $\tau$  the relaxation time), the relaxation time  $\tau$  is determined. The relaxation time for the  $\text{Li}_4\text{Ti}_5\text{O}_{12}$  and  $\text{Li}_4\text{Ti}_{2.5}\text{Cr}_{2.5}\text{O}_{12}$  are 1.8 and 0.07 ms, respectively. The reduced relaxation time is the proof for the high discharge rates of  $\text{Li}_4\text{Ti}_{2.5}\text{Cr}_{2.5}\text{O}_{12}$ .

The value of the FWHM in  $Z''$  vs  $\log f$  plots is shown in Fig. 11. A wider low-frequency peak, i.e., grain boundary peak, indicates that a distribution of relaxation time exists inside the grain boundaries. For a single relaxation time, the height of the peak in the  $Z''$  vs  $\log f$  plot must be equal to

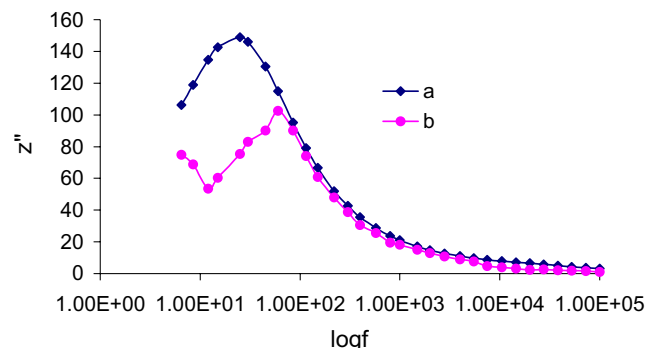


Fig. 11  $\log f$  vs  $Z''$ . *a*  $\text{Li}_4\text{Ti}_5\text{O}_{12}$ , *b*  $\text{Li}_4\text{Ti}_{2.5}\text{Cr}_{2.5}\text{O}_{12}$

half of the resistance value. In this sample, the height of the peak is lower than the value of the grain boundary resistance obtained from  $Z''$  versus  $Z'$  plots. This is attributed to overlapping of grains and grain boundary relaxation time.

Further, the dependence of the drift mobility,  $\mu$ , on the absolute temperature at different frequencies is calculated from the relation  $\sigma = ne\mu$  where  $n$  is number of charge carriers per unit volume and is given by the relation  $n = (NA\rho)/M$  where  $NA$  is the Avogadro number,  $\rho$  is the density, and  $M$  is the molecular weight of the sample,  $e$  is the electronic charge ( $1.6 \times 10^{-19}$  C). The mobility of  $\text{Li}_4\text{Ti}_5\text{O}_{12}$  and  $\text{Li}_4\text{Ti}_{2.5}\text{Cr}_{2.5}\text{O}_{12}$  are  $2.936 \times 10^{-6} \text{ cm}^2 \text{ V}^{-1} \text{ s}^{-1}$  and  $5.133 \times 10^{-6} \text{ cm}^2 \text{ V}^{-1} \text{ s}^{-1}$ , respectively, thus explaining the faster kinetics of  $\text{Li}_4\text{Ti}_{2.5}\text{Cr}_{2.5}\text{O}_{12}$ .

## Conclusion

Chromium-substituted  $\text{Li}_4\text{Ti}_5\text{O}_{12}$  was synthesized using the solid-state method followed by quenching. The minimum formation temperature required for  $\text{Li}_4\text{Ti}_{2.5}\text{Cr}_{2.5}\text{O}_{12}$  was around 600 °C. The discharge capacities of the  $\text{Li}_4\text{Ti}_{2.5}\text{Cr}_{2.5}\text{O}_{12}$  was much higher than those of the unsubstituted  $\text{Li}_4\text{Ti}_5\text{O}_{12}$  when the of rate of discharge was increased. The diffusion was increased by the chromium substitution. The conduction mechanism of the synthesized compound was explained through dielectric analysis, relaxation time ( $\tau$ ), and mobility ( $\mu$ ) of the compound. It is found that the conduction for Cr-substituted compound is of little higher than the parent, which was responsible for the high discharge rate.

**Acknowledgment** This work was carried out with the financial support from DRDO, India. The author thanks the Director of CECRI for his kind permission to publish this paper.

## References

- Colbow KM, Dahn JR, Haering RR (1989) *J Power Sources* 26:397
- Zaghib K, Armand M, Gauthier M (1998) *J Electrochem Soc* 145:3135
- Ohzuku T, Iwakoshi Y, Sawai K (1993) *J Electrochem Soc* 140:2490
- Nishisawa M, Hashitani R, Itoh T, Matsue T, Uchida I (1998) *Electrochem Solid-State Lett* 1:10–12
- Zaghib K, Simoneau M, Armand M, Gauthier M (1999) *J Power Sources* 81–82:300–305
- Guerfi A, Sevigny S, Lagace M, Hovington P, Kinoshita K, Zaghib K (2003) *J Power Sources* 119–121:88
- Scharner S, Weppner W, Schmid-Beurmann P (1999) *J Electrochem Soc* 146:857
- Thackeray MM, Johnson PJ, De Picciotto LA, Bruce PG, Goodenough JB (1984) *Mater Res Bull* 19:179
- Ohzuku T, Ueda A, Yamamoto N (1995) *J Electrochem Soc* 142:1431
- Peramunage D, Abraham KM (1998) *J Electrochem Soc* 145:2609
- Chen CH, Vaughey JT, Jansen AN, Dees DW, Kahaian AJ, Goacher T, Thackeray MM (2001) *J Electrochem Soc* 148:A102
- Robertson AD, Trevino L, Tukamoto H, Irvine JTS (1999) *J Power Sources* 81–82:352
- Robertson AD, Tukamoto H, Irvine JTS (1999) *J Electrochem Soc* 146:3958
- Sun YK, Jung DJ, Lee YS, Nahm KS (2004) *J Power Sources* 125:242–245
- Kavan L, Gratzel M (2002) *Electrochem Solid-State Lett* 5:A39
- Rho YH, Kanamura K, Umegaki T (2001) *Chem Lett*, p 1322
- Kanamura K, Umegaki T, Naito H, Takehara Z, Yao T (2001) *J Appl Electrochem* 31:73
- Bach S, Pereira-Ramos JP, Baffier N (1999) *J Power Sources* 81–82:273
- Peramunage D, Abraham KM (1998) *J Electrochem Soc* 145:2615
- Allen GC, Paul M (1995) *Appl Spectrosc* 49:451
- Ma S, Noguchi H (2001) *J Electrochem Soc* 148:A589
- Bach S, Pereira-Ramos JP, Baffier N (1998) *J Mater Chem* 8:251
- Kanamura K, Naito H, Takehara Z (1997) *Chem Lett*, p 45
- Thomas MGSR, Bruce PG, Goodenough JB (1985) *J Electrochem Soc* 132:1521
- Cabanel R, Barral G, Diard JP, Le Gorrec B, Montella C (1993) *J Appl Electrochem* 23:92
- Krtil P, Fattachova D (2001) *J Electrochem Soc* 148:A1045